Energy Storage Materials 49 (2022) 502–508

Contents lists available at ScienceDirect

Energy Storage Materials

journal homepage: www.elsevier.com/locate/ensm

Temperature and stress-resistant solid state electrolyte for stable lithium-metal batteries

Wenya Lei [a,1], Xingxing Jiao [a,1], Shugui Yang [a], Farshad Boorboor Ajdari [b], Masoud Salavati-Niasari [c], Yangyang Feng [a], Jianqing Yin [a], Goran Ungar [a], Jiangxuan Song [a,*]

[a] State Key Laboratory for Mechanical Behavior of Materials, Shaanxi International Research Center for Soft Matter, Xi'an Jiaotong University, Xi'an 710049, China
[b] Department of Applied Chemistry, Faculty of Chemistry, University of Kashan, Kashan 8731753153, Iran
[c] Institute of Nano Science and Nano Technology, University of Kashan, Kashan, P. O. Box. 87317-51167, I. R. Iran

ARTICLE INFO

Keywords:
Temperature and stress-resistance
Self-healing
Composite electrolyte
Solid state battery
Interface compatibility

ABSTRACT

Despite inherent good safety and high energy density, solid state batteries readily suffer from sudden capacity fading that stems from the structure deterioration under external/internal stress and temperature change. Herein, a temperature and stress-resistant solid-state battery is developed by utilizing a composite electrolyte, synthesized by chemically grafting a self-healing polyurethane-urea disulfide polymer (PUS) onto $Li_7P_3S_{11}$ via nucleophilic addition. In this way, $Li_7P_3S_{11}$ and PUS are kept in close contact ensuring their uniform distribution throughout the composite electrolyte. These chemically bound interfaces restrict PUS chain movement under cooling-heating cycling, and thus avoid phase separation in the composite electrolyte that often occurs in traditional systems. This ensures an unprecedented resilience of both capacity and conductivity (stable at 5×10^{-4} S cm^{-1}) to temperature fluctuations. Moreover, the dynamic S-S bond in PUS provides a fast self-healing rate of the composite electrolyte subjected to mechanical damage (100% current recovery within 3 min). The Li|PUS-LPS|$LiFePO_4$ full cell also displays super high post-damage capacity recovery of 95.1% and excellent cycling stability (95.4% capacity retention after 200 cycles).

1. Introduction

Lithium-ion batteries (LIBs) are widely used energy storage systems for various applications including electric vehicles, portable devices and smart electric grids [1–3]. However, the usage of liquid electrolytes in the commercial LIBs possess serious safety risks such as fire and explosion. Solid-state-batteries (SSEs) have drawn increasing attention as the next generation energy-storage systems due to their excellent thermal and electrochemical stability [4,5]. When coupled with lithium metal anode and high capacity/voltage cathode, the gravimetric energy density is expected to rise beyond 500 Wh/kg, twice as high as the contemporary state-of-the-art lithium-ion batteries [3]. There are mainly two kinds of solid state electrolytes for use in such batteries, i.e. ceramic (CEs) and polymer electrolytes (PEs) [6]. The former, such as garnet-type $Li_7La_3Zr_2O_{12}$, [7] NASCON-type $Li_{1.5}Al_{0.5}Ge_{1.5}(PO_4)_3$ [8] and $Li_7P_3S_{11}$, [9] exhibit relatively high ionic conductivity (>10^{-4} S cm^{-1}) and wide electrochemical potential window (0–6 V vs Li^+/Li) [10]. However, their practical application are impeded by their poor fracture toughness and high electrode interface impedance (Fig. 1a) [11]. Differently, PEs have excellent mechanical flexibility but usually show low ion conductivity (<10^{-5} S cm^{-1}) at room temperature [11,12]. To mitigate the above limitations of solo CEs or PEs, composite solid electrolytes, coupling appropriate soft organic PEs and stiff inorganic CEs, are in development, combining the advantages of both types [13]. Most of these developments are aimed at improving the ionic conductivity, electrode wettability and mechanical strength [14]. To improve these properties of composite solid electrolytes, preparation processes and electrolyte structure have been optimized. E.g. hot pressing and 3D printing have been used to produce structures such as polymer in ceramic or 3D ceramic networks [15].

Composite solid electrolytes are usually prepared by physical mixing methods such as solution casting or ball milling [15–18]. Although the introduction of the polymer component could enhance the flexibility of composite electrolyte, the irreversible damage and the phase separation still occur under the impact of destructive external forces or high temperature. In addition, mechanical stresses are also caused by large

* Corresponding author.
E-mail address: songjx@xjtu.edu.cn (J. Song).
[1] These authors contribute equally to this work

https://doi.org/10.1016/j.ensm.2022.04.015
Received 9 December 2021; Received in revised form 22 March 2022; Accepted 6 April 2022
Available online 10 April 2022

volume changes in the high-capacity electrode such as lithium metal (virtually infinite volume change) or silicon anode (up to 400% volume change) during cycling [19]. When paired with high specific capacity anodes, such as Li or Si, such volume changes inevitably cause cracks or fracture of the electrolyte [20–22], resulting in sudden capacity loss of the SSEs. This eventually leads to severe reduction in ionic conductivity (Fig. 1b) [20,21,23]. Recently, Zhang's group found that ionic conductivity of physically mixed LGPS-PEO/PEG composite electrolyte dropped significantly after high-temperature exposure, which was caused by the phase separation of ceramic and polymer phases, thereby greatly impeding the transport of lithium ions [24]. Although encouraging progress has been made in making composites more heat-resistant, few SSEs have reached practical application standards [5]. Furthermore, to cope with external mechanical damage, self-healing polymer electrolytes with different structures and repair efficiencies have been widely reported [22,25,26]. However, the study on self-healing composite electrolytes is lacking. Taking multi-scenario application into account, it is necessary to design a composite electrolyte with superior resistance to temperature and mechanical stress.

In this work, we have designed a novel type of composite electrolyte (denoted PUS-LPS), prepared by in-situ chemical grafting to build a bridge between LPS and polymer matrix (Fig. 1c). Therefore, LPS and PUS are linked through the P-N bond, which results in a composite electrolyte with stable structure that maintains stable ion conductivity under high temperatures. Moreover, the abundant dynamic disulfide bonds in the polymer chains endow the PUS-LPS composite with fast self-healing properties. Furthermore, the PUS-LPS can maintain stable ion channels even when mechanically damaged. Benefiting from these advantages, the $LiFePO_4$|Li full cell with PUS-LPS composite electrolyte shows high capacity and high capacity retention under harsh condition.

2. Results and discussion

2.1. Synthesis and characterizations of the PUS-LPS composite electrolyte

The PUS was synthesized by stepwise polymerization. The polyethylene glycol 2000 (PEG 2000)/isophorone diisocyanate (IPDI) ratio was optimized to maximize ionic conductivity and mechanical resilience [27,28]. 4,4′-Dithiodiphenylamine (DTDA) was selected as a chain extender containing plenty of aromatic disulfides bonds to endow the polymer with high self-healing ability (Figure S1 and Fig. 2a) [19,29]. The chemical structure of PUS is confirmed by infrared spectroscopy (FTIR) (Figure S2). In the PUS-LPS composite electrolyte, $Li_7P_3S_{11}$ (LPS, $70Li_2S$-$30P_2S_5$) was used as the inorganic component due to its high ionic conductivity and high chemical reactivity. Its identity was confirmed by comparing its powder X-ray diffractogram in Figure S3 with that in ref. [30]. The self-healing PUS-LPS composite electrolyte was prepared by heating and stirring lithium bis(fluorosulfonyl)imide (LiFSI), LPS and PUS polymer in argon atmosphere for 12 h, whereby PUS matrix and LPS ceramic particles are integrated through chemical bonds. The reaction was accompanied by obvious color change (Figure S4). As shown in Fig. 2b, LPS and PUS were tightly bound via the P-N bond through the nucleophilic addition reaction between the $P = S$ bond of $Li_7P_3S_{11}$ and $-NH_2$ group in the polymer chain. The chemical grafting between PUS and LPS particles is further confirmed by XPS and FTIR spectra shown in Figs. 2c-f and S5. In the P 2p spectrum of PUS-LPS

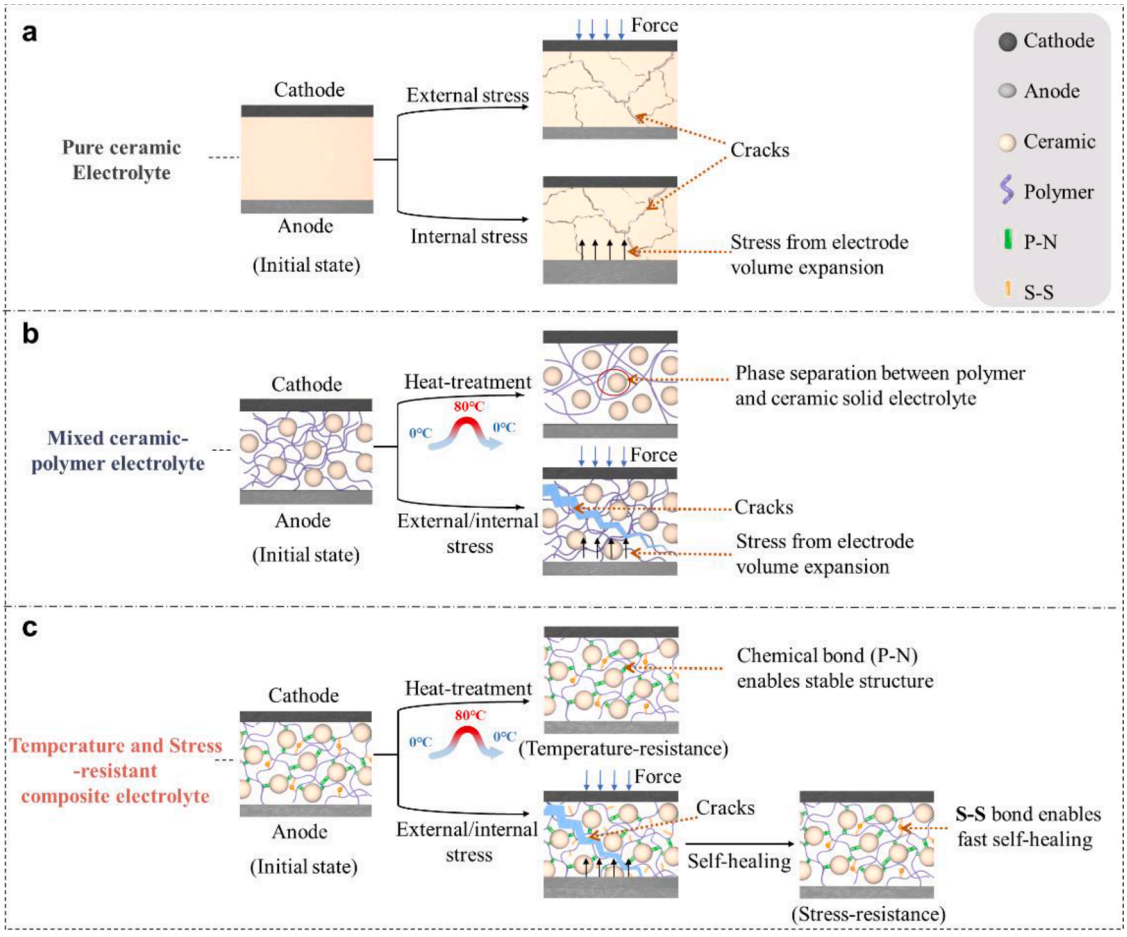

Fig. 1. Schematic of the behavior under harsh conditions of (a) ceramic electrolyte, (b) ceramic-polymer mixture and (c) temperature and stress-resistant composite electrolyte.

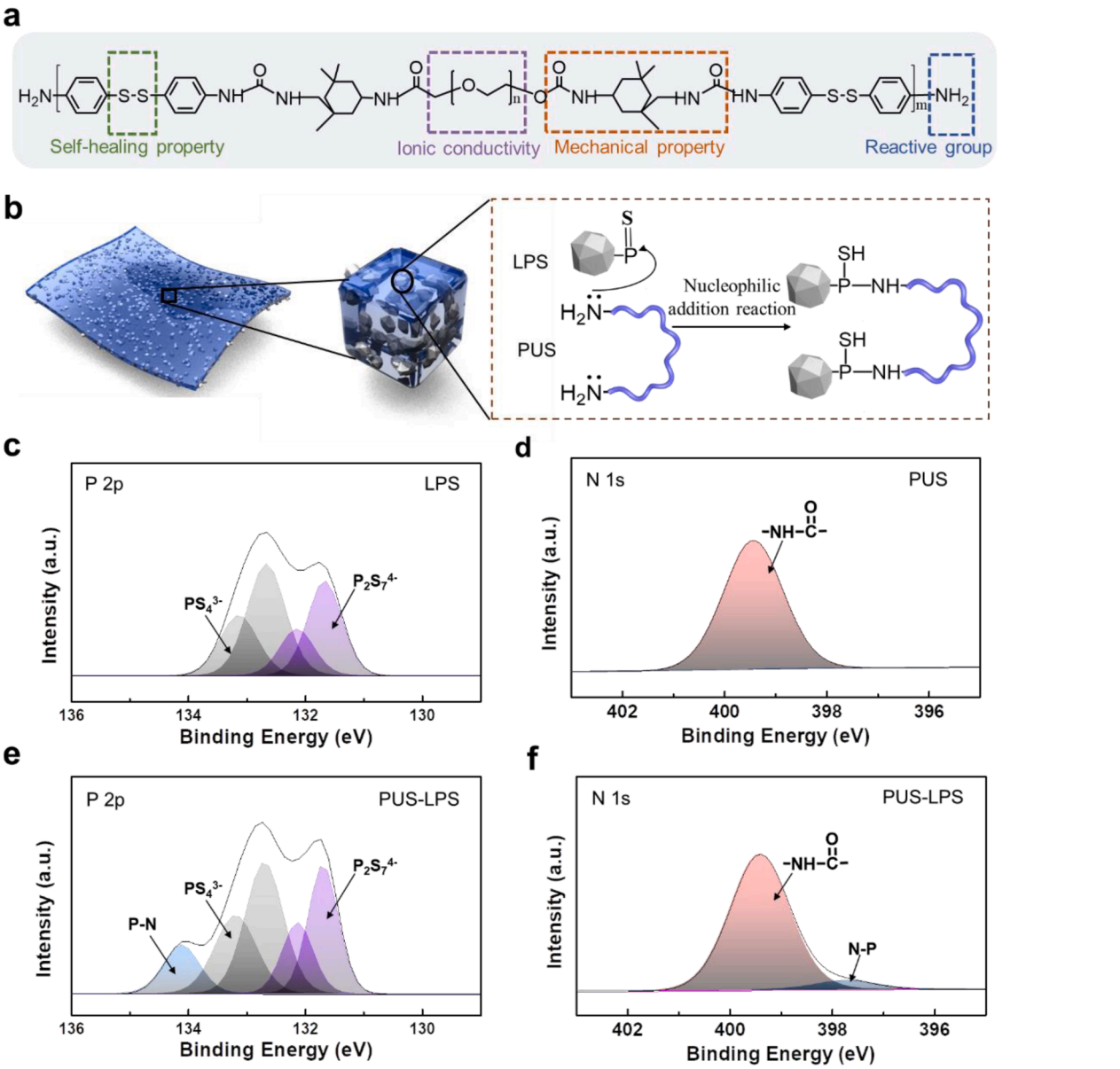

Fig. 2. Synthesis of temperature and stress -resistant composite solid electrolyte. (a) Molecular structure of PUS. (b) Schematic illustration of chemical grafting reaction between $Li_7P_3S_{11}$ and PUS. (c, e) P 2p and (d, f) N 1 s XPS spectra of LPS, PUS and PUS-LPS, respectively.

(Fig. 2e), the peak at 134.1 eV related to P-N is observed, which is the result of the reaction between PUS and LPS (Fig. 2c) [30,31]. As shown in Fig. 2d, the peak located at 399.5 eV corresponds to the -NH—CO- group in PUS, whereas a new peak at 397.6 eV appears in PUS-LPS (Fig. 2f), illustrating the formation of the P-N bond between LPS and the PUS [32]. More importantly, the original IR absorption peak at 1630 cm^{-1}, characteristic of $-NH_2$ groups in PUS, had disappeared after the addition of LPS (Figure S5), indicating that PUS and LPS were successfully connected via P-N chemical bridges.

The inset image in Fig. 3a shows the translucent PUS-LPS film with a thickness of ~28 μm, thinner than most composite electrolytes reported so far [13,33]. As shown in the SEM elemental mapping image in Fig. 3b, and the AFM image in Fig. 3c, the LPS particles with an average size of 2 μm (darker patches in Fig. 3c) are uniformly distributed in PUS. In contrast, for a reference electrolyte containing a PEO-LPS mixture (Figure S6), obvious micro-sized agglomerates (50 μm) and uneven distribution of LPS particles are observed. [34] Different dispersibility of LPS particles in the chemically bonded PUS-LPS composite and the physically mixed PEO-LPS composite clearly illustrates the benefit of chemical grafting in improving uniform dispersion of inorganic particles in a polymer electrolyte matrix [24,35]. The PUS-LPS membrane has a higher tensile strength of 2.1 MPa and a lower elongation at break of 1000% (Fig. 3d-e) compared to pure PUS membrane (Figure S7), which can substantially prolong the life of the PUS-LPS composite electrolyte. Fig. 3f shows that the Tg of PUS-LPS (−47 °C) is lower than that of pure PUS (−42 °C), which helps improve segment mobility [24] of PUS and facilitate the transport of lithium ions [12]. The formation of chemical bonds increases the crosslink density thus contributing to the increase of Tg [36]. On the other hand, the addition of inorganic solid electrolytes decreases the crystallinity of PEO, which in turn decreases the Tg [6,37,38]. Therefore, the combined effect of the two resaons causes a small increase in the Tg of PUS-LPS. As shown in Figure S8, the PUS-LPS shows negligible weight loss until the temperature up to 260 °C (99.02 wt%), confirming that very little residual solvent (< 1 wt%) in the PUS-LPS. This makes the ionic conductivity independent of the solvent and confirms the good thermal stability of the PUS-LPS electrolyte.

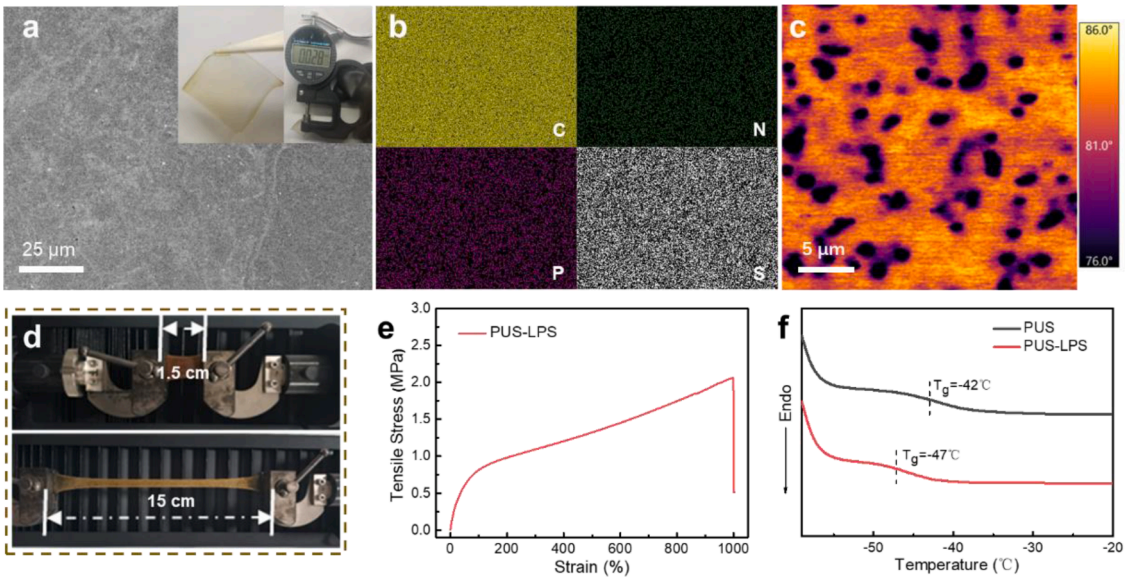

Fig. 3. Physical properties of PUS-LPS. (a) SEM image and (b) corresponding EDS element mapping (C, N, P and S) of PUS-LPS membrane (Inset: photograph of a PUS-LPS membrane). (c) AFM images for PUS-LPS. (d) Optical image of PUS-LPS membrane tensile test. (e) Stress-strain curve of PUS-LPS membrane. (f) DSC heating curves of PUS and PUS-LPS.

2.2. Temperature-resistance of the PUS-LPS composite electrolyte

The effect of LPS and LiFSI content on the ionic conductivity of the as-prepared PUS-LPS was also investigated (Figure S9 and Figure S10). The optimized PUS-LPS composite electrolyte of 7 wt% LPS at the optimal EO/Li ratio of 10:1 shows high ionic conductivities of 5×10^{-4} S cm^{-1} and 4.7×10^{-3} S cm^{-1} at 25 °C and 80 °C, respectively. In addition, PUS-LPS membrane has the lithium ion transfer number (t_{Li}^{+}) of about 0.49 (Figure S11) and an electrochemical stability window of about 4.8 V (Figure S12).

The ionic conductivities of PEO-LPS and PUS-LPS membranes were measured using electrochemical impedance spectroscopy (EIS). As shown in Fig. 4a and d, after treating at 80 °C for 1 h, the chemically grafted PUS-LPS composite electrolyte shows relatively stable ionic conductivity, while the ionic conductivity of PEO-LPS mixture decreases from 8.3×10^{-6} S cm^{-1} to 4.9×10^{-6} S cm^{-1}. X-ray powder diffraction (XRD) and polarizing optical microscope were further used to identify crystal textures of composite electrolytes upon heat treatment. Figure S13 shows sharp diffraction peaks at $2\theta = 19$ and 23.5°, assigned to crystalline of PEO in PEO-LPS mixture. While, PUS-LPS sample shows a broad diffraction peak without any detectable sharp peaks (Figure R3a), further indicating that the amorphous structure of PUS-LPS electrolyte. PUS-LPS display amorphous phase without birefringent spherulites before and after heat treatment (Fig. 4b-c), while PEO-LPS mixture shows obvious birefringent spherulites (Fig. 4e-f). The spherulites of PEO-LPS become larger and the spherulites boundaries grow more blurred after thermal treatment compared to the initial state. As shown in Figure S14, DSC curves of PUS-LPS exhibit no melting peak

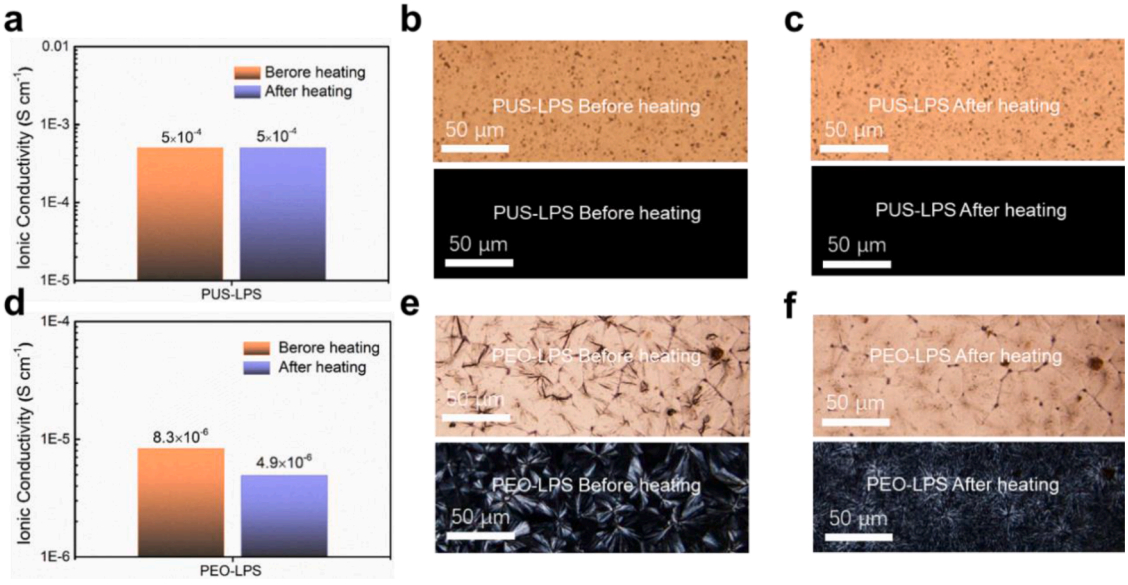

Fig. 4. Temperature-resistance of the PUS-LPS. (a) Ionic conductivity of PUS-LPS measured before and after exposure to 80 °C for 2 h. (b-c) Optical micrographs images of PUS-LPS before and after heating at 80 °C (The upper half of the image: bright field; The bottom half of the image: polarized optical microscopy). (d) Ionic conductivity test of PEO-LPS before and after heating at 80 °C. (e-f) Optical microscopy images of PEO-LPS before and after heating at 80 °C (The upper half of the image: bright field; The bottom half of the image: polarized optical microscopy).

upon heating to 100 °C and no recrystallization peaks under cooling to 10 °C. Moreover, compared with PUS-LPS, the DSC curves of PEO-LPS exhibit melting peak upon heating and recrystallization peaks under cooling, which again confirms its high crystallinity nature. This spherulites and morphology change for PEO-LPS strongly indicates the movement and rearrangement of polymer segments, causing PEO/LPS phase separation. Therefore, the separation phase of PEO-LPS mixture between the ceramic and the polymer phase after heat treatment results in destruction of lithium ion conduction pathways at the organic-inorganic interface, which can significantly lower ionic conductivity [37]. In contrast, the P-N bond in the PUS-LPS composite electrolyte binds the polymer to the ceramic surface preserving the beneficial interfaces.

2.3. Stress-resistance of the PUS-LPS composite electrolyte

Stress-resistance of the solid electrolyte is an important prerequisite for safe battery operation, Figs. 5a-c show the self-healing behavior of PUS-LPS. The electrolyte was firstly cut in two with a knife. When put back in contact at room temperature, the PUS-LPS film heals within 3 min (Fig. 5c). This is attributed to the continuous dynamic breaking and reforming of the disulfide bonds (-S-S-) [29]. Furthermore, after scratching with a sharp object PUS-LPS can self-heal at room temperature within 5 min leaving only a slight trace (Figure S15a-c). The healing ability of PUS-LPS composite is comparable to that of pure PUS (Figure S15d-f). The self-healing process was schematically shown in Figure S16. In order to evaluate the self-healing ability of PUS-LPS in battery-like environment, the experimental device in Fig. 5d was applied. The current was monitored over time before and after damage under an alternating voltage of ±2 V [23]. Fig. 5e shows the current alternating between ±6.5 μA in the original state and then dropping to ±2.7 μA after cutting at 25 °C. The current is seen to recover to ±6.5 μA after mere ~2.7 min without any external force. The corresponding current curve shows that the PUS-LPS recovers to ~100% of the initial current within only 163 s at 25 °C (Fig. 5f). Therefore, the results confirm the ability of the electrolyte to quickly self-repair ruptures caused by internal stresses (such as electrode volume change) or external forces. This self-healing ability will ensure stable battery operation.

2.4. Electrochemical performance of Li cells with PUS-LPS composite electrolyte

The interface stability of PUS-LPS with lithium metal anode was also analyzed by a galvanostatic cycling experiment on symmetric Li|PUS-LPS|Li cells. In Fig. 6a-b, the PUS-LPS-equipped symmetric Li cells exhibited stable voltage profiles (50 and 90 mV) over 600 h and 400 h under a current density of 0.2 mA cm^{-2} (with areal capacity of 0.1 mAh cm^{-2}) and 0.5 mA cm^{-2} (with areal capacity of 1 mAh cm^{-2}) at 25 °C. In order to observe the interface on the lithium anode, SEM image was performed to reveal the morphology of lithium anode after 50 cycles at 0.5 mA cm^{-2}. From the surface and cross-sectional view (Figure S17) it can be seen that the lithium metal has smooth and dense morphology, indicating that the interface on the lithium anode is stable and free of dendrites. The EIS spectra of symmetric cells (Figure S18) after various shelving times further demonstrate the high stability of this interface. XPS spectra (Figure S19) show that the SEI layer on the surface of Li anode is rich in LiF and Li_3N. In order to demonstrate the application of the PUS-LPS composite electrolyte in a full, Li|PUS-LPS|$LiFePO_4$ cell, such a cell was assembled and tested at different rates. The capacity of the battery was initially 125.8 mAh g^{-1} at 0.5 C, and it still remained as high as 117.2 mAh g^{-1} after 300 cycles (Fig. 6c). The discharge-charge curve of the Li|PUS-LPS|LFP cells shows almost no polarization change after 300 cycles (Figure S20), indicating that the interface is fairly stable during cycling. Although the discharge capacity decreases slightly with the increase of current density, the full Li|PUS-LPS|LFP cell still maintain a high capacity of 140.5, 134.8, 124.7, and 107.6 mAh g^{-1} at 0.1, 0.3, 0.5, and 1.0 C, respectively (Fig. S21).

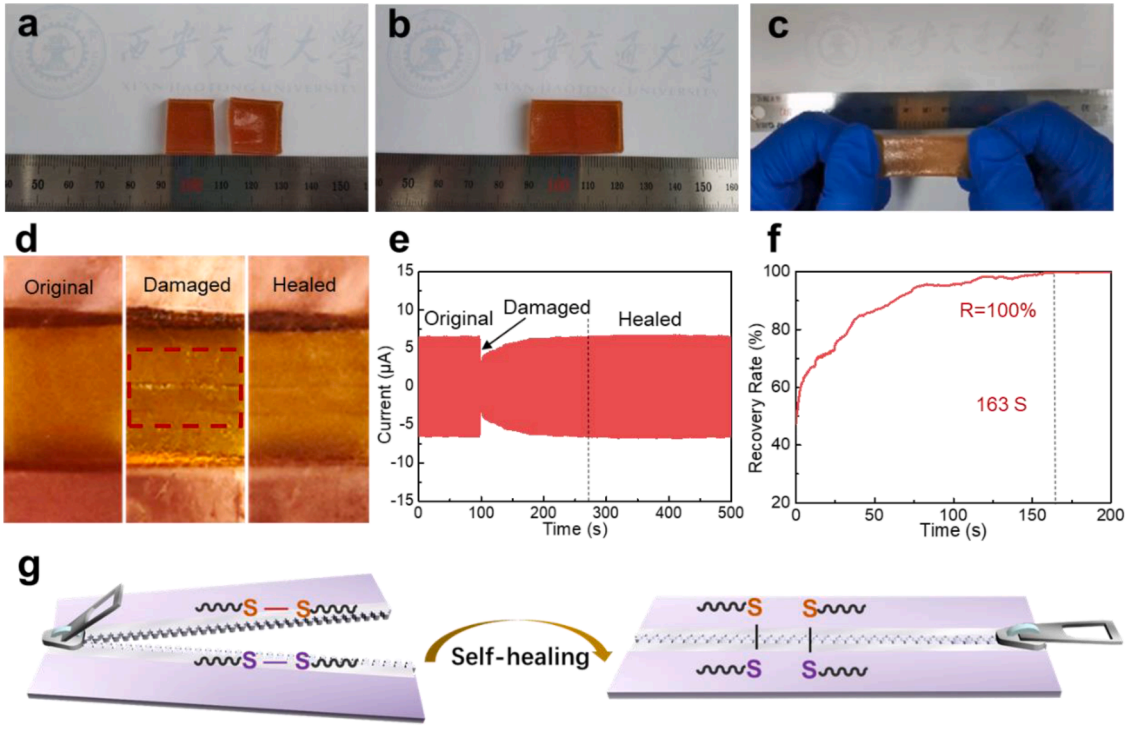

Fig. 5. Stress-resistance of PUS-LPS. (a) Optical images of PUS-LPS electrolyte film mechanically cut in half, (b) put back into contact, and (c) subjected to tensile test after 5 min healing at 25 °C. (d) Optical images of the original, mechanically damaged, and healed PUS-LPS sample on the Cu collector at 25 °C. (e) Time-dependence of current under an alternating voltage of ±2 V before and after PUS-LPS was cut with a ceramic blade at 25 °C (oscilloscope display). (f) Currents recovery at 25 °C (from experiment in e). (g) Proposed schematic of the healing process.

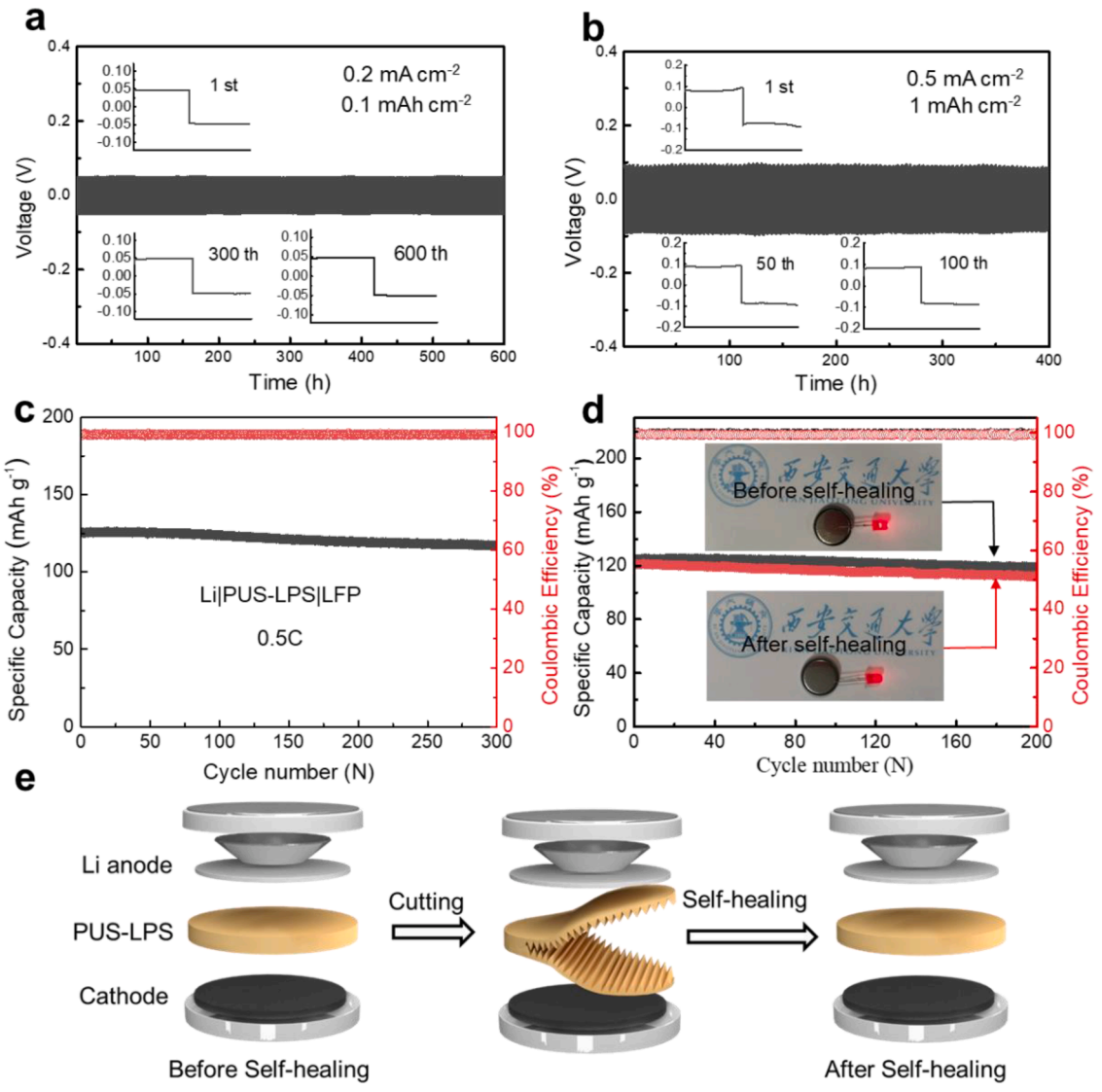

Fig. 6. Electrochemical performance of Li cells with PUS-LPS. Cycling stability of a typical symmetric Li|PUS-LPS|Li cell at current density of (a) 0.2 mA cm^{-2} for 0.1 mAh cm^{-2} capacity and (b) 0.5 mA cm^{-2} for 1 mAh cm^{-2} capacity. (c) Cycling performance of Li|PUS-LPS|$LiFePO_4$ cells cycled at a rate of 0.5 C. (d) Cycling performance of Li|PUS-LPS|$LiFePO_4$ cells cycled before and after self-healing (Inset: photographs of a LED light before and after self-healing test). (e) Schematic diagram of a Li|PUS-LPS|$LiFePO_4$ coin cell test of self-healing.

In order to demonstrate the stress-resistance of the full cell, the PUS-LPS film was cut in two (Fig. 6e and Figure S22). After that, the two pieces were put together. The reassembled battery was still able to light up the LED (see inset in Fig. 6d). By contrast, the PEO-LPS electrolyte failed the test (Figure S23). Significantly, Li|PUS-LPS|$LiFePO_4$ cells have been shown to exhibit good cycling stability with only 4.6% decrease of capacity after the damage and high post-damage capacity recovery of 95.1% (Fig. 6d). Moreover, the Li|PUS-LPS|$LiFePO_4$ cells display a smaller interface impedance compared with the Li|PEO-LPS|$LiFePO_4$ (Figure S24). The results confirm that the PUS-LPS, containing a multitude of reversible disulfide bonds, can effectively recover the integrity of the electrode after damage. The full Li|PUS-LPS|$LiFPO_4$ cell displays a high capacity of 126 mAh g^{-1} under 25 °C. As the temperature increases to 60 °C, the capacity increases to 145 mAh g^{-1}. In addition, the capacity of the battery recovers to 125 mAh g^{-1} after the temperature returning to 25 °C. Moreover, the cell shows an initial capacity of 146 mAh g^{-1} at 0.5 C and a capacity retention of 95.6% after 80 cycles under 60 °C (Figure S25).

3. Conclusion

In summary, we have designed a temperature and stress-resistant solid electrolyte (PUS-LPS) consisting of a disulphide-containing polyurethane-urea matrix with chemically bonded $Li_7P_3S_{11}$ ceramic microparticles. The P-N bond in the PUS-LPS composite electrolyte ensures unprecedented resilience of both capacity and ionic conductivity against temperature fluctuations. In addition, the dynamic nature of the "living" S-S bond in the polymer ensures fast self-healing of the PUS-LPS electrolyte when damaged mechanically; ~100% current recovery is achieved within only 2.7 min at 25 °C. These properties have proven highly effective in maintaining stability of the electrolyte structure. Furthermore, the full Li|PUS-LPS|$LiFePO_4$ cell exhibits extraordinarily high post-damage capacity recovery of 95.1% and excellent cycling stability (95.4% capacity retention after 200 cycles). The good ionic conductivity and high temperature- and stress-resistance incorporated in our PUS-LPS electrolyte promises a successful solution for safe and reliable solid-state batteries.

CRediT authorship contribution statement

Wenya Lei: Formal analysis, Investigation, Methodology, Writing – original draft, Writing – review & editing. **Xingxing Jiao:** Formal analysis, Methodology, Writing – original draft, Writing – review & editing. **Shugui Yang:** Methodology. **Farshad Boorboor Ajdari:** Formal analysis. **Masoud Salavati-Niasari:** Writing – review & editing. **Yangyang Feng:** Writing – review & editing. **Jianqing Yin:** Formal analysis. **Goran Ungar:** Formal analysis, Writing – review & editing. **Jiangxuan Song:** Conceptualization, Supervision, Funding acquisition, Project administration, Writing – review & editing.

Declaration of Competing Interest

The authors declare that they have no known competing financial interests or personal relationships that could have appeared to influence the work reported in this paper.

Data Availability

Data will be made available on request.

Acknowledgements

This work is supported by the National Natural Science Foundation of China (No. 21875181), the 111 Project 2.0 of China (BP2018008), Key Research and Development Program of Shaanxi (2019TSLGY07–05), Natural Science Basic Research Program of Shaanxi (No.2019JLP-13). We would like to thank Miss Liu at the Instrument Analysis Center of Xi'an Jiaotong University for her assistance with XPS analysis. We also thank Senior Engineer Wei Wang at state key laboratory for mechanical behavior of materials for SEM measurements.

Supplementary materials

Supplementary material associated with this article can be found, in the online version, at doi:10.1016/j.ensm.2022.04.015.

References

[1] P. Oh, H. Lee, S. Park, H. Cha, J. Kim, J. Cho, Improvements to the overpotential of all-solid-state lithium-ion batteries during the past ten years, Adv. Energy Mater. 10 (2020), 2000904.
[2] K. Liu, X. Li, J. Cai, Z. Yang, Z. Chen, B. Key, Z. Zhang, T.L. Dzwiniel, C. Liao, Design of high-voltage stable hybrid electrolyte with an ultrahigh li transference number, ACS Energy Lett. (2021) 1315–1323.
[3] W.P. Chen, H. Duan, J.L. Shi, Y. Qian, J. Wan, X.D. Zhang, H. Sheng, B. Guan, R. Wen, Y.X. Yin, S. Xin, Y.G. Guo, L.J. Wan, Bridging interparticle Li(+) conduction in a soft ceramic oxide electrolyte, J. Am. Chem. Soc. 143 (2021) 5717–5726.
[4] Z. Zou, Y. Li, Z. Lu, D. Wang, Y. Cui, B. Guo, Y. Li, X. Liang, J. Feng, H. Li, C. W. Nan, M. Armand, L. Chen, K. Xu, S. Shi, Mobile ions in composite solids, Chem. Rev. 120 (2020) 4169–4221.
[5] L.-.Z. Fan, H. He, C.-.W. Nan, Tailoring inorganic–polymer composites for the mass production of solid-state batteries, Nat. Rev. Mater. (2021) 1003–1019.
[6] G. Cui, Reasonable design of high-energy-density solid-state lithium-metal batteries, Matter 2 (2020) 805–815.
[7] H. Xie, Y. Bao, J. Cheng, C. Wang, E.M. Hitz, C. Yang, Z. Liang, Y. Zhou, S. He, T. Li, L. Hu, Flexible garnet solid-state electrolyte membranes enabled by tile-and-grout design, ACS Energy Lett. 4 (2019) 2668–2674.
[8] S. Xiong, Y. Liu, P. Jankowski, Q. Liu, F. Nitze, K. Xie, J. Song, A. Matic, Design of a multifunctional interlayer for nascion-based solid-state li metal batteries, Adv. Funct. Mater. 30 (2020), 2001444.
[9] G.-.L. Zhu, C.-.Z. Zhao, H. Yuan, B.-.C. Zhao, L.-.P. Hou, X.-.B. Cheng, H.-.X. Nan, Y. Lu, J. Zhang, J.-.Q. Huang, Q.-.B. Liu, C.-.X. He, Q. Zhang, Interfacial redox behaviors of sulfide electrolytes in fast-charging all-solid-state lithium metal batteries, Energy Stor. Mater. 31 (2020) 267–273.
[10] H.W. Kim, J. Han, Y.J. Lim, Y. Choi, E. Lee, Y. Kim, 3d Ion-conducting, scalable, and mechanically reinforced ceramic film for high voltage solid-state batteries, Adv. Funct. Mater (2020), 2002008.
[11] L. Chen, X. Qiu, Z. Bai, L.-.Z. Fan, Enhancing interfacial stability in solid-state lithium batteries with polymer/garnet solid electrolyte and composite cathode framework, J. Energy Chem. 52 (2021) 210–217.
[12] H. Wang, Q. Wang, X. Cao, Y. He, K. Wu, J. Yang, H. Zhou, W. Liu, X. Sun, Thiol-branched solid polymer electrolyte featuring high strength, toughness, and lithium ionic conductivity for lithium-metal batteries, Adv. Mater. (2020), e2001259.
[13] T. Jiang, P. He, G. Wang, Y. Shen, C.W. Nan, L.Z. Fan, Solvent-free synthesis of thin, flexible, nonflammable garnet-based composite solid electrolyte for all-solid-state lithium batteries, Adv Energy Mater 10 (2020), 1903376.
[14] D.H.S. Tan, A. Banerjee, Z. Chen, Y.S. Meng, From nanoscale interface characterization to sustainable energy storage using all-solid-state batteries, Nat. Nanotechnol. 15 (2020) 170–180.
[15] J. Liang, J. Luo, Q. Sun, X. Yang, R. Li, X. Sun, Recent progress on solid-state hybrid electrolytes for solid-state lithium batteries, Energy Storage Mater. 21 (2019) 308–334.
[16] N. Boaretto, L. Meabe, M. Martinez-Ibañez, M. Armand, H. Zhang, Review—polymer electrolytes for rechargeable batteries: from nanocomposite to nanohybrid, J. Electrochem. Soc. 167 (2020), 070524.
[17] J.-.F. Wu, X. Guo, Mof-derived nanoporous multifunctional fillers enhancing the performances of polymer electrolytes for solid-state lithium batteries, J. Mater. Chem. A 7 (2019) 2653–2659.
[18] M. Liu, Z. Cheng, S. Ganapathy, C. Wang, L.A. Haverkate, M. Tułodziecki, S. Unnikrishnan, M. Wagemaker, Tandem Interface and bulk Li-ion transport in a hybrid solid electrolyte with microsized active filler, ACS Energy Lett 4 (2019) 2336–2342.
[19] X. Jiao, J. Yin, X. Xu, J. Wang, Y. Liu, S. Xiong, Q. Zhang, J. Song, Highly energy-dissipative, fast self-healing binder for stable Si anode in lithium-ion batteries, Adv. Funct. Mater. (2020), 2005699.
[20] B. Zhou, Y.H. Jo, R. Wang, D. He, X. Zhou, X. Xie, Z. Xue, Self-healing composite polymer electrolyte formed via supramolecular networks for high-performance lithium-ion batteries, J. Mater. Chem. A 7 (2019) 10354–10362.
[21] Y.H. Jo, B. Zhou, K. Jiang, S. Li, C. Zuo, H. Gan, D. He, X. Zhou, Z. Xue, Self-healing and shape-memory solid polymer electrolytes with high mechanical strength facilitated by a Poly(vinyl alcohol) matrix, Polym. Chem. 10 (2019) 6561–6569.
[22] W. Mai, Q. Yu, C. Han, F. Kang, B. Li, Self-healing materials for energy-storage devices, Adv. Funct. Mater. 30 (2020), 1909912.
[23] B.B. Jing, C.M. Evans, Catalyst-free dynamic networks for recyclable, self-healing solid polymer electrolytes, J. Am. Chem. Soc. 141 (2019) 18932–18937.
[24] K. Pan, L. Zhang, W. Qian, X. Wu, K. Dong, H. Zhang, S. Zhang, A flexible ceramic/polymer hybrid solid electrolyte for solid-state lithium metal batteries, Adv. Mater. 32 (2020), e2000399.
[25] J. Xu, C. Ding, P. Chen, L. Tan, C. Chen, J. Fu, Intrinsic self-healing polymers for advanced lithium-based batteries: advances and strategies, Applied Physics Reviews 7 (2020), 031304.
[26] R. Narayan, C. Laberty-Robert, J. Pelta, J.M. Tarascon, R. Dominko, Self-healing: an emerging technology for next-generation smart batteries, Adv. Energy Mater. (2021), 2102652.
[27] J. Xu, J. Chen, Y. Zhang, T. Liu, J. Fu, A fast room-temperature self-healing glassy polyurethane, Angew Chem Int Ed Engl 60 (2021) 7947–7955.
[28] S.-.M. Kim, H. Jeon, S.-.H. Shin, S.-.A. Park, J. Jegal, S.Y. Hwang, D.X. Oh, J. Park, Superior toughness and fast self-healing at room temperature engineered by transparent elastomers, Adv. Mater. 30 (2018).
[29] A. Rekondo, R. Martin, A. Ruiz de Luzuriaga, G. Cabañero, H.J. Grande, I. Odriozola, Catalyst-free room-temperature self-healing elastomers based on aromatic disulfide metathesis, Mater. Horiz. 1 (2014) 237–240.
[30] S. Wenzel, D.A. Weber, T. Leichtweiss, M.R. Busche, J. Sann, J. Janek, Interphase formation and degradation of charge transfer kinetics between a lithium metal anode and highly crystalline Li7p3s11 solid electrolyte, Solid State Ion 286 (2016) 24–33.
[31] J. Wu, X. Zheng, C. Jin, J. Tian, R. Yang, Ternary doping of phosphorus, nitrogen, and sulfur into porous carbon for enhancing electrocatalytic oxygen reduction, Carbon 92 (2015) 327–338.
[32] I. Villaluenga, K.H. Wujcik, W. Tong, D. Devaux, D.H.C. Wong, J.M. DeSimone, N. P. Balsara, Compliant glass-polymer hybrid single ion-conducting electrolytes for lithium batteries, PNAS 113 (2016) 52–57.
[33] J. Wan, J. Xie, X. Kong, Z. Liu, K. Liu, F. Shi, A. Pei, H. Chen, W. Chen, J. Chen, X. Zhang, L. Zong, J. Wang, L.Q. Chen, J. Qin, Y. Cui, Ultrathin, flexible, solid polymer composite electrolyte enabled with aligned nanoporous host for lithium batteries, Nat. Nanotechnol. (2019) 705.
[34] S. Xia, J. Lopez, C. Liang, Z. Zhang, Z. Bao, Y. Cui, W. Liu, High-rate and large-capacity lithium metal anode enabled by volume conformal and self-healable composite polymer electrolyte, Adv. Sci. (2019), 1802353.
[35] F.Y. Shen, M.B. Dixit, X.H. Xiao, K.B. Hatzell, Effect of pore connectivity on Li dendrite propagation within Llzo electrolytes observed with synchrotron X-ray tomography, ACS Energy Lett. 3 (2018) 1056–1061.
[36] K. Bandzierz, L. Reuvekamp, J. Dryzek, W. Dierkes, A. Blume, D. Bielinski, Influence of network structure on glass transition temperature of elastomers, Materials (Basel) 9 (2016).
[37] L. Chen, Y. Li, S.-.P. Li, L.-.Z. Fan, C.-.W. Nan, J.B. Goodenough, Peo/Garnet composite electrolytes for solid-state lithium batteries: from "ceramic-in-polymer" to "polymer-in-ceramic, Nano Energy 46 (2018) 176–184.
[38] Y. Zhao, Z. Huang, S. Chen, B. Chen, J. Yang, Q. Zhang, F. Ding, Y. Chen, X. Xu, A promising Peo/Lagp hybrid electrolyte prepared by a simple method for all-solid-state lithium batteries, Solid State Ionics 295 (2016) 65–71.